

**Shock compression response of diamond single crystals at multimegabar stresses**J. M. Winey <sup>1</sup>, M. D. Knudson <sup>1,2</sup> and Y. M. Gupta <sup>1</sup><sup>1</sup>*Institute for Shock Physics and Department of Physics, Washington State University, Pullman, Washington 99164-2816, USA*<sup>2</sup>*Sandia National Laboratories, Albuquerque, New Mexico 87185-1195, USA*

(Received 16 September 2019; revised manuscript received 17 April 2020; accepted 21 April 2020; published 8 May 2020)

Shock compressed diamond response at multimegabar stresses—of fundamental interest to high pressure science and relevant for high energy density experiments related to inertial confinement fusion—is often assumed to be hydrodynamic. To examine this assumption, plate impact experiments were conducted to measure wave profiles in diamond single crystals shocked to  $\sim 900$  GPa elastic impact stress (EIS). For the [110] and [111] orientations, two-wave structures (elastic-inelastic response) were observed to  $\sim 900$  GPa EIS; in contrast, single (overdriven) waves were observed at 480 GPa EIS and above for the [100] orientation. The elastic wave velocities for the [110] and [111] orientations were significantly larger than those for the [100] orientation. Strong orientation dependence was also observed for the elastic wave amplitudes; for [110] and [111] diamond, the amplitudes increased significantly with increasing elastic impact stress. The observed two-wave structures and the strong orientation dependence (elastic wave speeds and amplitudes) demonstrate unequivocally that the shock response of diamond single crystals is not hydrodynamic at stresses below the melt transition. As such, appropriate elastic-inelastic material descriptions are needed to accurately model the high stress response of diamond and other strong solids.

DOI: [10.1103/PhysRevB.101.184105](https://doi.org/10.1103/PhysRevB.101.184105)**I. INTRODUCTION**

Scientific studies using shock wave experiments were pioneered in the 1950s, both in the United States and in the Soviet Union [1–5]. In these early experiments, conducted using high explosive drivers, shock velocity and free surface velocity measurements were often used to characterize the shock compressed state. Together with the Rankine-Hugoniot jump conditions [1,2], these measurements were sufficient to determine the longitudinal stress ( $P_x$ )–volume ( $V$ ) states in materials subjected to extreme compressions. These measured states, referred to as the Hugoniot data, were central to examining and understanding the thermodynamic response of materials at extreme conditions not attainable using other methods. These early studies provided an excellent foundation for shock wave studies in the following six decades that have significantly expanded the compression range of shock experiments.

The earliest experimental studies were undertaken on polycrystalline metals (isotropic solids) and the Hugoniot data were utilized for thermodynamic studies by assuming a hydrodynamic response for the shocked state [1,2]. The hydrodynamic approximation can be rigorously defined as follows: the lateral stresses ( $P_y = P_z$ ), which do not appear in the conservation equations for plane shock compression and, as such, cannot be obtained from the usual measurements, are assumed to be equal to the longitudinal stress ( $P_x$ ). Using this approximation,  $P_x$  is identified as the thermodynamic pressure ( $P$ ). Much of the shock wave literature, particularly at high stresses, has utilized this assumption.

In 1961, Fowles' measurements on aluminum showed the existence of a two-wave structure resulting from shock wave

induced elastic-plastic deformation arising from the stress difference  $P_x \neq P_y (=P_z)$  [6]. The schematic representation in Fig. 1 is commonly assumed in the elastic-plastic deformation analysis of shock wave data from Fowles and subsequent workers. The hydrodynamic approximation is invalid when the deviatoric stress ( $P_x - P_{\text{mean}}$ ) (related to the stress difference  $P_x - P_y$ ) cannot be ignored. Fowles' results demonstrated that the hydrodynamic assumption is not valid in solids, at least at moderate stresses [6]. Since 1961, various approaches have been developed to extract thermodynamic information from elastic-plastic deformation in shock compressed solids. References [6–8] can be consulted for further discussion of this topic. With the subsequent development of various time-resolved methods [9] to measure propagating shock wave profiles in materials [10–13], elastic-plastic deformation studies under shock wave compression have been undertaken in a very wide range of solids, mostly at peak shock stresses below a Mbar (100 GPa) [14–20].

At higher stresses (above a Mbar), wave profile measurements are sparse and shock data are commonly analyzed by using impedance matching [2,5], along with the hydrodynamic assumption. The hydrodynamic approximation at high stresses has been justified on the grounds that the deviatoric stresses (related to material strength) in the shocked state are negligible compared to the peak longitudinal stress ( $P_x$ ) [1]. This assumption is convenient for utilizing the shock data for thermodynamic studies, including equation of state development, of materials at extreme conditions. Although high stress shock wave data have been, and continue to be, most commonly analyzed using the hydrodynamic approximation, it should be emphasized that the quantity determined from the experiments is  $P_x$  and not  $P$ . By utilizing novel

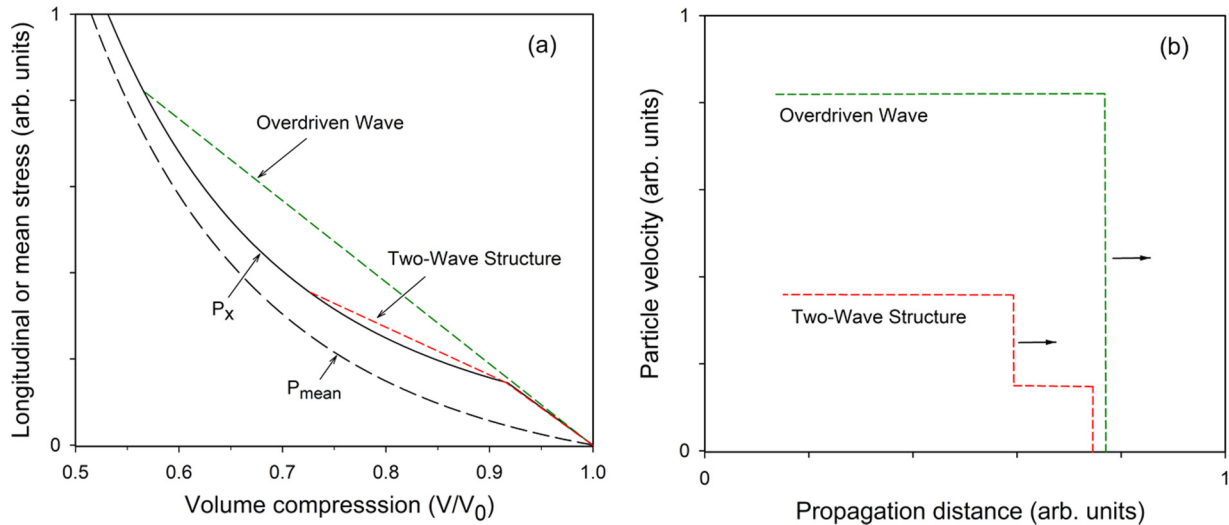


FIG. 1. Schematic representation commonly assumed for the elastic-plastic deformation analysis of shock-compressed solids. In panel (a), the black solid and dashed curves are the longitudinal and mean stress curves, respectively. The green dashed curve and the red dashed curve represent the Rayleigh lines for an overdriven wave and two-wave structure, respectively. Panel (b) shows a schematic time snapshot of the propagating waves that correspond to the Rayleigh lines in panel (a).

experimental approaches, extreme thermophysical conditions in bulk matter can now be accessed and shock data are widely used to understand thermodynamic states relevant to high pressure phenomena in a broad range of physical science disciplines (condensed matter physics/chemistry [5,17,21–24], high energy density science including fusion related studies [25–27], materials science [14,16,28,29], and geo/planetary science [15,30,31]).

Although the hydrodynamic assumption may be reasonable for metals and many other types of solids at very high shock stresses—due to the concomitant increase in temperature—the validity of this assumption for strong and stiff materials remains an unresolved scientific issue. The shock compression response of diamond, the archetypal strong solid, is of particular interest in this regard. Because shock wave results in diamond samples, below the melting stress, have often been analyzed assuming a hydrodynamic response [32–35], the following conceptual questions are of significant importance: at what stresses would the hydrodynamic assumption be valid for diamond, how would crystal anisotropy be manifested at multi-Mbar stresses in shocked diamond, and how to understand and model the inelastic response of diamond at these very high stresses if the hydrodynamic assumption is invalid?

Motivated by the above questions, we present experimental results for diamond single crystals shocked to multi-Mbar stresses. Two features of our experimental work are noteworthy: the use of plate impact experiments to ensure well defined initial conditions and the use of sufficiently thick samples (0.9 mm) to achieve high precision shock velocity measurements. The present experiments have significantly exceeded the stresses attained in previous plate impact experiments on diamond single crystals [32,36–38] and the present results clearly demonstrate that the hydrodynamic assumption is not valid for diamonds shocked to the very high stresses attained in the present work.

The remainder of the paper is organized as follows. The experimental methods are summarized in Sec. II. Experimental results, including determination of elastic-inelastic shock wave structures and elastic wave speeds, are presented in Sec. III. In Sec. IV, the experimental results are analyzed and discussed regarding the hydrodynamic assumption and regarding earlier studies. The main findings of this work are summarized in Sec. V.

## II. EXPERIMENTAL METHODS

### A. Diamond single crystals

The synthetic diamond single crystals used in the present experiments were grown by chemical vapor deposition (CVD) and were polished to an optical finish. The polished crystals were colorless, without observable defects, and were used as received from Element Six. Using x-ray diffraction, the orientation of each crystal was determined to be within 1–3° of the desired orientation. Sample thicknesses were measured to within 1  $\mu\text{m}$  using both optical (through-the-lens laser auto focus instrument) and mechanical (two-point-contact micrometer) measurements. Lateral dimensions were nominally 4.0 and 4.5 mm square for the 500- and 900- $\mu\text{m}$  samples, respectively. The density of the diamond samples was determined using high precision measurements of mass and dimensions; the average and standard deviation were found to be 3.50 and 0.02  $\text{g}/\text{cm}^3$ , respectively. Thus, the CVD diamond samples used in this study were determined to be at full theoretical density within measurement error.

### B. Plate impact experiments

Plate impact experiments were conducted at the Z pulsed power facility [39] at Sandia National Laboratories, Albuquerque, using the experimental configurations shown schematically in Figs. 2 and 3. Composite copper/aluminum

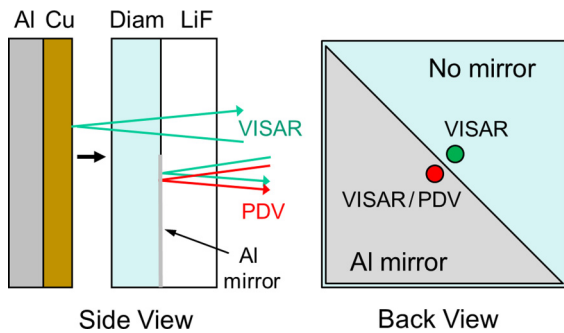


FIG. 2. Configuration for experiments incorporating diamond single crystals backed by [100]-oriented LiF windows. The back view shows the positioning of the interferometer probes and the Al mirror.

flyer plates, launched using the magnetic drive generated by the Z machine [40], were impacted on targets consisting of a diamond single crystal backed by an optical window ([100]-oriented lithium fluoride or *z*-cut quartz). Both the diamond samples and the windows (either LiF or quartz) had one surface with antireflection (AR) coating for 532 nm. The LiF windows had a triangular half coating of aluminum ( $\sim 400$ -nm thick) deposited on the side opposite the AR coating (Fig. 2). The diamond samples and windows were bonded together using a low-viscosity epoxy (Angstrombond) with bond thicknesses on the order of  $1 \mu\text{m}$  or less. These sample stacks were then bonded into a target frame holder, similar to that described in Ref. [31]. The two target frames, each holding up to seven sample stacks, were mounted into experimental load panels such that the impact surfaces of the diamond samples were at a prescribed flight distance from the composite Cu/Al flyer plate (typically 3–4 mm, depending upon the desired impact velocity).

Laser interferometry—both VISAR (Velocity Interferometer System for Any Reflector, 532 nm) [13,41] and PDV (Photonic Doppler Velocimetry, 1550 nm) [42,43]—was used to measure the velocity of reflective surfaces in the target (such as the Cu flyer plate surface, the aluminum coating at the diamond/LiF interface, or the quartz shock front) and to determine the shock wave transit times in the diamond sample. Typical velocity per fringe settings for the VISAR ranged from 404.5 to 2289.5 m/s/fringe. Multiple PDV diagnostics

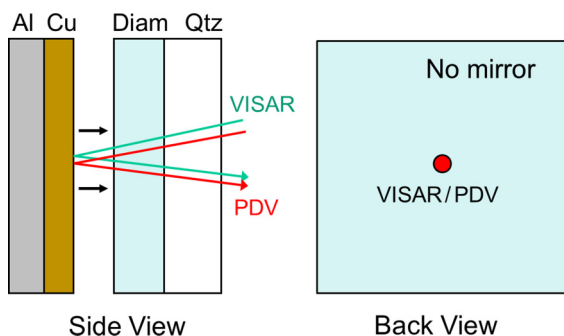


FIG. 3. Configuration for experiments incorporating diamond single crystals backed by *z*-cut quartz windows. The back view shows the positioning of the interferometer probes.

were used for each shot and were run in both standard and heterodyne configuration, enabling apparent velocity measurements that spanned from rest to over 50 km/s. Diamond samples backed by LiF windows were configured with two probes, as shown in Fig. 2: (1) a VISAR probe positioned approximately 0.5 mm away from the sample stack diagonal such that the laser light passed through the LiF window and diamond sample to the flyer plate impact surface, and (2) a combination VISAR/PDV probe positioned approximately 0.5 mm away from the other side of the sample stack diagonal such that the laser light reflected off the aluminum coating at the diamond/LiF interface. Diamond samples backed by quartz windows were configured with a single combination VISAR/PDV probe positioned at the center of the sample stack (Fig. 3). Laser light from these probes passed through the quartz window and diamond sample to the flyer plate impact surface. Interferometry data (both VISAR and PDV) from experiments that incorporated LiF windows were analyzed using the window corrections from Ref. [44]. Window corrections were not required for the experiments that incorporated quartz windows.

### III. RESULTS

The Z experiments conducted in the present work resulted in impact velocities ranging from 9.5 km/s to 15.3 km/s. Six diamond single crystals were impacted in each experiment: three different crystal orientations were examined ([100], [110], and [111]), with two different sample thicknesses (nominally  $500 \mu\text{m}$  and  $900 \mu\text{m}$ ) for each orientation. The relevant experimental parameters for each diamond sample are listed in Table I.

Representative interferometry results for an experiment having a LiF window (Z3203–S10) are shown in Fig. 4. The measured flyer velocity is observed until the time of impact. At impact, the interferometer signal is lost due to shock-induced optical opacity in the diamond crystal. The shock wave arrival at the back of the diamond sample is indicated by a jump in velocity at the diamond/LiF interface. These measurements provide the shock wave transit time through the diamond sample, resulting in a determination of the shock wave velocity.

At higher impact velocities, the peak stress in the LiF window exceeds the optical transmission limit for shocked LiF [44]; for these experiments, a *z*-cut quartz window was used [31]. Figure 5 shows representative interferometry results for an experiment that incorporated a quartz window (Z3029–S7). Similar to the experiments using a LiF window, the time of impact is indicated by the loss of interferometer signal in the flyer velocity profile. Subsequent recovery of the interferometer signal indicates the arrival of the shock wave at the diamond/quartz interface because, at the peak stresses reached in the experiments presented here, the shock wave in the quartz window is reflective [45]. Thus, the interferometer signal recovery provides the shock wave transit time through the diamond, resulting in a determination of the shock wave velocity in diamond. Furthermore, due to the shock front reflectivity in diamond, the interferometer provides a direct measurement of the quartz shock velocity history. Although the quartz shock velocity is related, in principle,

TABLE I. Experimental parameters.

Shot/sample number	Diamond crystal orientation	Window	Sample thickness ( $\mu\text{m}$ )	Impact velocity (km/s)
Z3203-N4	[100]	[100] LiF	$468 \pm 1$	9.500
Z3203-N10	[100]	[100] LiF	$948 \pm 1$	9.525
Z3203-N7	[110]	[100] LiF	$531 \pm 1$	9.536
Z3203-S7	[110]	[100] LiF	$922 \pm 1$	9.624
Z3203-S4	[111]	[100] LiF	$546 \pm 1$	9.622
Z3203-S10	[111]	[100] LiF	$904 \pm 1$	9.657
Z3116-S3	[100]	z Quartz	$479 \pm 1$	10.91
Z3116-S7	[100]	[100] LiF	$945 \pm 1$	11.01
Z3116-S5	[110]	z Quartz	$518 \pm 1$	10.88
Z3116-N5	[110]	[100] LiF	$942 \pm 1$	10.87
Z3116-N3	[111]	z Quartz	$546 \pm 1$	10.86
Z3116-N7	[111]	[100] LiF	$912 \pm 1$	10.97
Z3029-S3	[100]	z Quartz	$469 \pm 1$	12.22
Z3029-S7	[100]	z Quartz	$947 \pm 1$	12.40
Z3029-S5	[110]	z Quartz	$474 \pm 1$	12.23
Z3029-N5	[110]	z Quartz	$945 \pm 1$	12.22
Z3029-N3	[111]	z Quartz	$537 \pm 1$	12.20
Z3029-N7	[111]	z Quartz	$914 \pm 1$	12.34
Z3011-S3	[100]	z Quartz	$459 \pm 1$	15.21
Z3011-S7	[100]	z Quartz	$913 \pm 1$	15.31
Z3011-S5	[110]	z Quartz	$530 \pm 1$	15.25
Z3011-N5	[110]	z Quartz	$947 \pm 1$	15.26
Z3011-N3	[111]	z Quartz	$456 \pm 1$	15.25
Z3011-N7	[111]	z Quartz	$923 \pm 1$	15.30

to the shocked state in the diamond, the analysis required to relate the two is challenging and cannot be carried out

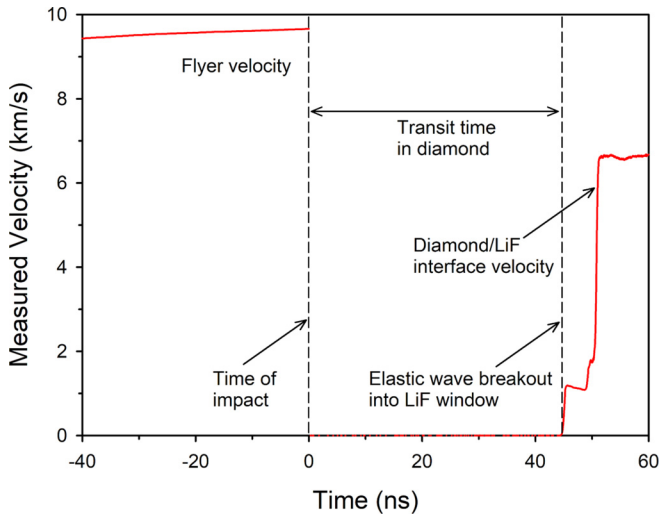


FIG. 4. Representative results for plate impact experiments on diamond single crystals backed by a LiF window. Laser interferometry results from experiment Z3203-S10 show the flyer velocity up until impact, loss of signal upon impact with the diamond sample, and arrival of the shock wave at the diamond/LiF interface. For the results shown here, the measured diamond/LiF interface velocity indicates a two-wave structured shock.

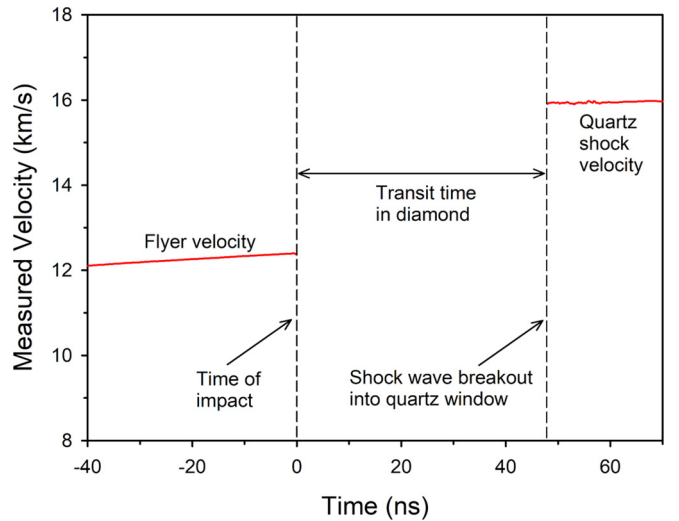


FIG. 5. Representative results for plate impact experiments on diamond single crystals backed by a quartz window. Laser interferometry results from experiment Z3029-S7 show the flyer velocity up until impact, loss of signal upon impact with the diamond sample, and recovery of signal when the shock wave breaks out of the diamond and into the quartz window. For the results shown here, the measurements indicate a single, overdriven shock wave in the diamond.

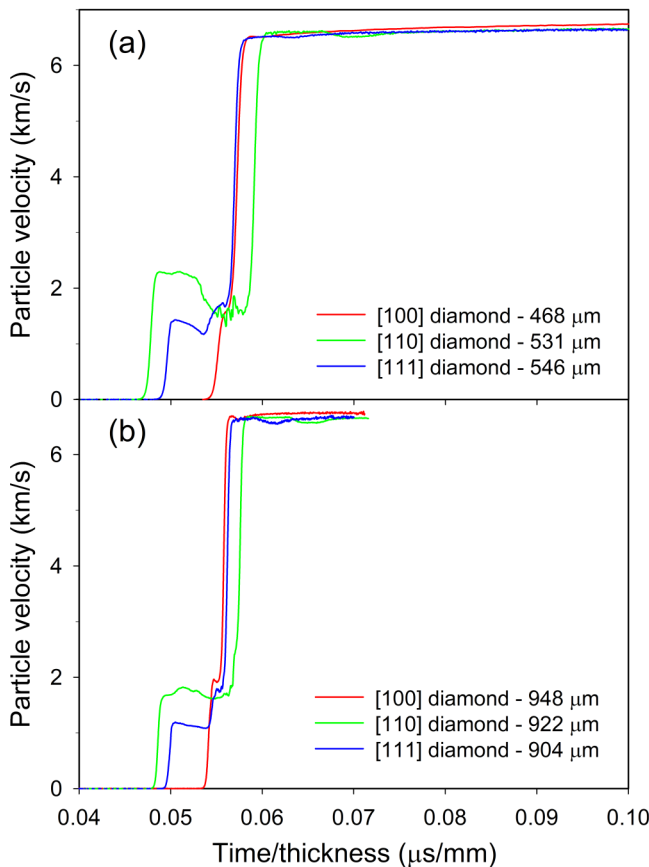


FIG. 6. Particle velocity profiles measured at the diamond/LiF interface for (a) 500- $\mu\text{m}$ -thick diamond and (b) 900- $\mu\text{m}$ -thick diamond for experiment Z3203. Time is relative to impact and the time axes are normalized by the sample thickness to better compare the measured profiles. Note that VISAR fringe ambiguities in the elastic waves for the two [100] diamond profiles were resolved using the elastic wave amplitudes from Table II.

reliably without an accurate material model for diamond. Such a model is currently under development.

For diamond single crystals shocked to stresses beyond the elastic limit, two different shock wave structures are possible: two-wave structure (elastic-inelastic response) or single-wave structure (elastic wave overdriven). The shock wave structure for each diamond sample was determined using laser interferometry measurements. For experiments incorporating a LiF window, the measured wave profile provides a direct indication of the shock wave structure. Figure 4 shows a representative measured wave profile having a two-wave structure; the elastic wave arrives first and the subsequent arrival of the inelastic wave takes the material to the peak state. For experiments incorporating a quartz window, determination of the shock wave structure is more involved and is described in the Appendix. Figure 5 shows a representative measurement from a quartz window experiment that resulted in a single overdriven wave in the diamond.

Measurements from experiments resulting in a two-wave structure for the three diamond single crystal orientations are the focus of the present manuscript. Figure 6 shows the wave profiles measured in shot Z3203, which incorporated a LiF

window. All six of the profiles show a two-wave structure resulting from the elastic-inelastic response. However, the arrival time and interface velocity amplitude of the elastic waves differ significantly for the three crystal orientations.

The measured elastic wave speeds from all the experiments are listed in Table II and are shown in Fig. 7(a) as a function of the elastic impact stress (the stress attained at impact, assuming purely elastic diamond response). The elastic impact stress (EIS) can be determined accurately in plate impact experiments and provides a convenient parameter to compare results from experiments along different diamond orientations and at different stress inputs. The EIS was determined for each diamond sample by impedance matching [2,5] using the nonlinear elastic response of diamond single crystals discussed in Sec. IV A, together with the Hugoniot curve for copper [46] and the measured flyer velocities.

Figure 7(a) shows that the measured elastic wave speeds are highest for [110] diamond and wave speeds for [100] diamond are significantly lower compared to the other two orientations. Two-wave structures were observed for [110] and [111] diamond up to the highest stresses examined ( $\sim 900$  GPa EIS). In contrast, single overdriven waves were observed for [100] diamond at 480 GPa EIS and above, demonstrating significant orientation dependence for diamond single crystals shocked to high stresses.

A single overdriven wave was also observed for the 900- $\mu\text{m}$  [111] sample at  $\sim 900$  GPa (shot Z3011). The overdriven shock front in this sample was found to be slightly reflective (few percent reflectivity). Previous laser-shock studies on natural type IIa diamond [47] and quartz [45] have associated shock front reflectivity with melting at high stresses. Therefore, our results suggest solid/liquid coexistence in the 900- $\mu\text{m}$  [111] sample shocked to  $\sim 900$  GPa EIS. As discussed in the Supplemental Material [48] (see Fig. S1),  $\sim 900$  GPa EIS in [111] diamond corresponds to  $\sim 700$  GPa impact stress as determined using the Hugoniot curve for polycrystalline diamond [34]; this impact stress is comparable to melting stresses reported previously for shocked diamond [34,49]. We note that a reflective shock front was not observed for any of the other diamond samples in shot Z3011; for those samples, the peak stresses and temperatures likely approached, but did not reach, the conditions for melting onset.

## IV. ANALYSIS AND DISCUSSION

### A. Determination of elastic wave amplitudes

To enable determination of elastic wave amplitudes (from the measured elastic wave speeds) and determination of elastic impact stresses, nonlinear elastic stress-volume curves were determined for each diamond orientation using elastic wave amplitude data for shocked diamond published previously [50]. The published elastic stress-volume states for each orientation were fit using

$$P_x = -\frac{V_0}{V} \left\{ C'_{11} e_x + \frac{1}{2} C'_{111} e_x^2 \right\}, \quad (1)$$

where  $P_x$  is the longitudinal Cauchy stress (positive in compression),  $C'_{11}$  and  $C'_{111}$  are second-order and third-order elastic constants, and the uniaxial elastic strain is defined using a

TABLE II. Experimental results for elastic waves.

Shot/sample number	Diamond crystal orientation	Elastic impact stress (GPa)	Elastic wave velocity (km/s) <sup>a</sup>	Elastic wave amplitude (GPa) <sup>a,b</sup>	Elastic compression (V/V <sub>0</sub> ) <sup>a,b</sup>
Z3203–N4	[100]	394	18.1 ± 0.4	53.8 ± 32	0.9535 ± 0.001
Z3203–N10	[100]	395	18.4 ± 0.2	81.4 ± 17	0.9319 ± 0.0007
Z3203–N7	[110]	448	20.9 ± 0.4	109 ± 21	0.9293 ± 0.001
Z3203–S7	[110]	454	20.6 ± 0.2	92.8 ± 11	0.9377 ± 0.0007
Z3203–S4	[111]	454	20.1 ± 0.4	65.3 ± 18	0.9542 ± 0.0009
Z3203–S10	[111]	456	20.1 ± 0.2	62.6 ± 10	0.9559 ± 0.0005
Z3116–S3	[100]	475	Overdriven	Overdriven	Overdriven
Z3116–S7	[100]	481	Overdriven	Overdriven	Overdriven
Z3116–S5	[110]	540	21.4 ± 0.4	134 ± 24	0.917 ± 0.002
Z3116–N5	[110]	540	NA	NA	NA
Z3116–N3	[111]	539	NA	NA	NA
Z3116–N7	[111]	546	20.2 ± 0.2	66.6 ± 10	0.9534 ± 0.0005
Z3029–S3	[100]	555	Overdriven	Overdriven	Overdriven
Z3029–S7	[100]	566	Overdriven	Overdriven	Overdriven
Z3029–S5	[110]	639	21.6 ± 0.5	147 ± 28	0.911 ± 0.002
Z3029–N5	[110]	639	21.9 ± 0.3	160 ± 14	0.905 ± 0.001
Z3029–N3	[111]	636	20.8 ± 0.4	97 ± 21	0.936 ± 0.001
Z3029–N7	[111]	647	20.6 ± 0.2	88 ± 12	0.941 ± 0.001
Z3011–S3	[100]	755	Overdriven	Overdriven	Overdriven
Z3011–S7	[100]	762	Overdriven	Overdriven	Overdriven
Z3011–S5	[110]	884	22.6 ± 0.5	205 ± 33	0.887 ± 0.003
Z3011–N5	[110]	885	22.3 ± 0.3	186 ± 15	0.894 ± 0.001
Z3011–N3	[111]	883	22.1 ± 0.5	169 ± 33	0.902 ± 0.002
Z3011–N7	[111]	887	Overdriven	Overdriven	Overdriven

<sup>a</sup>As noted in the Fig. 7 caption, the experimental uncertainties for the 500-mm-thick diamond samples are approximately twice those of the 900-mm-thick samples.

<sup>b</sup>Determined using the nonlinear elastic response of diamond single crystals, as described in Sec. IV A.

logarithmic strain measure [51]

$$e_x = \ln(V/V_0). \quad (2)$$

In Eqs. (1) and (2),  $P_x$ ,  $e_x$ ,  $C'_{11}$ , and  $C'_{111}$  are defined relative to a coordinate system aligned with the direction of shock compression. The second-order elastic constant  $C'_{11}$  for each orientation was determined from diamond elastic constants measured previously [52]. The previously measured stress-strain states [50] were fit by adjusting only the third-order elastic constant  $C'_{111}$ . We note that the logarithmic strain formulation was chosen because it provides significantly better extrapolation behavior at high stresses, compared to more conventional formulations [51]. Because  $C'_{11}$  is known precisely for each orientation, the primary uncertainty in the nonlinear elastic formulation is associated with the determination of  $C'_{111}$ . The  $C'_{11}$  and  $C'_{111}$  values determined for each diamond orientation are shown in Table III, together with their associated uncertainties.

The resulting stress-volume curves for diamond shocked along the [100], [110], and [111] orientations are shown in Fig. 8, together with the previously published stress-volume states [50]. The results show that the above logarithmic strain formulation, shown in Eqs. (1) and (2), provides a useful

framework for extrapolating the nonlinear elastic response of diamond to higher stresses.

The elastic wave amplitude for each diamond sample was determined from the measured elastic wave speed using the following procedure. The nonlinear elastic stress-volume curves from Fig. 8 were converted to shock velocity ( $U_S$ ) – particle velocity ( $u_p$ ) relations using the Rankine-Hugoniot jump conditions [2,5]. The resulting nonlinear  $U_S$ – $u_p$  relations were used in conjunction with the measured elastic wave speeds ( $U_S$ ) to determine the in-material particle velocity for the elastically compressed state of each diamond sample. The Rankine-Hugoniot jump conditions were then used to determine the in-material longitudinal elastic stress and volume.

The results for each diamond sample are listed in Table II. The uncertainties for the longitudinal stresses and volumes depend primarily on the uncertainty in the elastic wave speed measurements and were determined by calculating upper and lower bounds. We note that determination of the elastic wave amplitudes required only modest extrapolations from the elastic stress-strain states measured previously for shocked diamond single crystals [50].

Figure 7(b) shows the elastic wave amplitudes as a function of the EIS. The elastic wave amplitudes for [110] diamond are

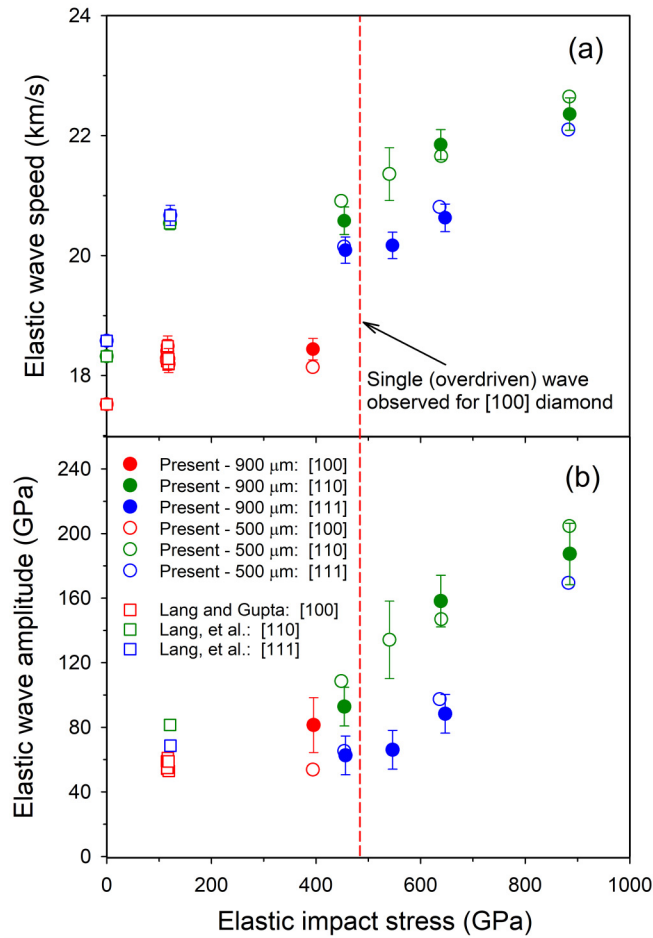


FIG. 7. (a) Elastic wave speed and (b) elastic wave amplitude versus elastic impact stress for diamond single crystals. The circles represent the present high stress results and the squares represent previous low stress results [36,37]. The open and solid symbols correspond to nominally 500- $\mu\text{m}$ - and 900- $\mu\text{m}$ -thick samples, respectively. The ambient sound speeds were determined from published elastic constants [52]. The elastic wave amplitudes were determined using the measured elastic wave speeds, together with the extrapolated nonlinear elastic response for each orientation (see Sec. IV A). The extrapolated nonlinear elastic response was also used to determine the elastic impact stresses. We note that the experimental precision, as expected, for wave velocity measurements on the 900- $\mu\text{m}$ -thick samples is almost twice that for the 500- $\mu\text{m}$ -thick samples. For visual clarity, the error bars are omitted for all but one of the measurements using the 500- $\mu\text{m}$ -thick samples. Uncertainties for all the measured values are listed in Table II. We note that, because the low stress experiments incorporated 500- $\mu\text{m}$ -thick samples only, it is possible that the uncertainties for the corresponding elastic wave speed measurements might have been underestimated in the previous work [36,37].

significantly larger than those for [100] and [111] diamond. In addition, Fig. 7(b) shows that the elastic wave amplitudes for [110] and [111] diamond increase considerably with increasing elastic impact stress.

Figure 7 also shows results from previous plate impact experiments by Lang *et al.* [36,37] at  $\sim 120$  GPa EIS. Overall, the previously measured wave speeds and amplitudes at  $\sim 120$

TABLE III. Parameters for Eq. (1). The  $C'_{11}$  values are from Ref. [52].

Diamond orientation	$C'_{11}$ (GPa)	$C'_{111}$ (GPa)
[100]	$1079 \pm 5$	$90 \pm 160$
[110]	$1180 \pm 7$	$-5400 \pm 670$
[111]	$1213 \pm 8$	$-5070 \pm 490$

GPa EIS are comparable to the present results at  $\sim 400$  GPa EIS, within the experimental uncertainties. Lang *et al.* previously showed that the elastic wave amplitudes were smaller for larger elastic impact stresses for stresses up to  $\sim 120$  GPa [37]. However, the results presented here suggest that while this trend may persist between  $\sim 120$  and  $\sim 400$  GPa EIS, the trend reverses at higher stresses.

## B. Findings and discussion regarding the hydrodynamic approximation

The present high stress results, together with the lower stress results reported previously [36,37], show that the elastic wave speeds, elastic wave amplitudes, and observed shock wave structures are all strongly dependent on crystal orientation. In addition, the results for [110] and [111] diamond show a two-wave structure (elastic-inelastic response), in which the elastic wave amplitude increases with increasing elastic impact stress, to stresses at or near the melting stress. These findings demonstrate unequivocally that the hydrodynamic approximation is not valid for diamond shocked to stresses below melt.

Although the present paper is focused on experimental results that show a two-wave structure, we note that the propagation of a single shock wave—as occurs for the [100] orientation at 480 GPa EIS and above—does not imply that

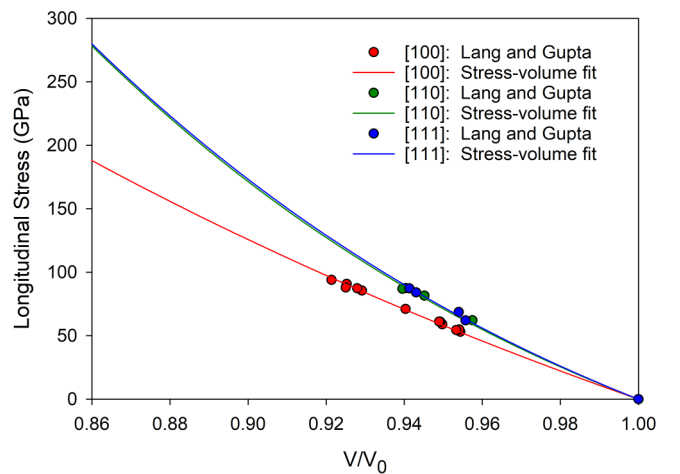


FIG. 8. Extrapolated nonlinear elastic response for diamond shock-compressed along the [100] orientation (red curve), [110] orientation (green curve), and [111] orientation (blue curve). The symbols are measured elastic compression states for shocked diamond single crystals [50]. Note that the extrapolated responses for [110] and [111] diamond are similar.

the hydrodynamic approximation is valid. As shown in Fig. 1, the final state reached through an overdriven wave can still support large deviatoric stresses ( $P_x - P_{\text{mean}}$ ). A single shock wave is merely a consequence of the fact that the end states can be connected by a single jump—the inelastic (or second) wave speed is higher than the elastic wave speed, resulting in an overdriven wave.

We also note that, in contrast to studies on isotropic solids, high stress shock wave studies in single crystals are quite sparse and rigorous analysis of shock wave data is challenging, as discussed in Refs. [53,54]. If the shock response along different crystal orientations is markedly different—as is the case for the diamond results presented here—even coming up with an equivalent definition corresponding to the “hydrodynamic approximation” used for isotropic solids is conceptually difficult. Although a longitudinal stress ( $P_x$ )–volume ( $V$ ) relation always exists for shock propagation along a given crystal orientation, the  $P_x - V$  relation is not unique and depends on the crystal orientation. Furthermore, the longitudinal and lateral stress differences vary with the crystal orientation and involve different elasticity tensor terms. Depending on the crystal orientation, the two lateral stresses may not even be identical.

While a mean stress  $(P_x + P_y + P_z)/3$  can always be written down for purely elastic deformation, determining the mean stress for elastic-inelastic deformation, in general, is not possible. Additional assumptions and/or information about the tensor nature of inelastic deformation (including a mathematical description of the deformation mechanism) are required. Simply put, measured two-wave structures and/or an overdriven wave cannot be simulated for a shocked single crystal without a complete description of an accurate material model. For a strong brittle solid like diamond, the development of a credible material model (incorporating inelastic deformation) is a major undertaking because traditional material modeling approaches, developed for isotropic materials, cannot provide an accurate description of the strongly anisotropic single crystal response [48]. However, obtaining high quality shock wave data along different crystal orientations, the focus of this paper, represents an important step in this direction.

### C. Comparison with laser-shock experiments

As noted previously [36,37], plate impact experiments on diamond differ significantly from previous laser-shock experiments reported in [55] with regard to: loading methods and durations, determination of input stresses, experimental precision, and sample purity. These differences are briefly discussed below (see also Ref. [48]).

(1) Loading methods and durations: Laser drive loading methods, such as those in Ref. [55], generate shock waves by depositing laser energy at the boundary of a target package. As a result, the shock stress can be sustained only for the duration of the laser pulse, placing strong limitations on the loading durations that can be achieved. For example, the longest loading duration achieved in Ref. [55] was about 6 ns. In contrast, loading at the impact surface is maintained for  $>300$  ns in the present plate impact experiments.

(2) Determination of input stresses: In contrast to the well-defined initial conditions encountered in plate impact

experiments, the laser-matter interactions that lead to the development of a laser-driven shock wave are complex and estimating the input stresses in the sample is not straightforward. As such, elastic impact stresses cannot be directly assigned to the previous laser-shock results [55]. Therefore, the elastic wave speeds and amplitudes from Ref. [55] cannot be compared on an equal footing with those presented here.

(3) Experimental precision: The above limitations on the loading duration placed limitations on the sample thicknesses that could be used in the laser-shock experiments; for example, the largest samples used in quasisteady wave experiments were  $\sim 200\text{-}\mu\text{m}$  thick [55]. Because the precision of measured wave transit times in the sample scales linearly with sample thickness, the small sample thicknesses used in Ref. [55] resulted in corresponding limitations on the precision of the elastic wave velocity measurements and, as noted in Ref. [50], the same, due to the large scatter, were not usable in the determination of the third order elastic constants of diamond. In contrast, the largest sample thicknesses used in the experiments presented here were  $\sim 900\text{-}\mu\text{m}$  thick, resulting in increased precision for the measured elastic wave velocities.

(4) Sample purity: Most of the diamond single crystals used in the previous laser shock experiments were type Ia natural diamonds [55], which have a significantly higher nitrogen content compared to the type IIa natural diamonds used by Lang *et al.* [36,37] and the CVD diamonds used in the experiments presented here.

Due to the above differences, it is difficult to compare the results presented here with those from Ref. [55], except for a few qualitative comments. Overall, the elastic wave velocities and elastic wave amplitudes reported in Ref. [55] increase somewhat with increasing peak stresses, in qualitative agreement with the trend presented here. However, the elastic wave velocities in Ref. [55] show relatively weak orientation dependence, in contrast to the strong orientation dependence presented here. In addition, two-wave structures were reported at relatively high peak stresses for all three diamond orientations [55], suggesting that the elastic waves for all three orientations were overdriven at similar stresses. In contrast, the results presented here show that the elastic wave for [100] diamond is overdriven at much lower stresses, compared to the other two orientations. Thus, the above comparison shows that the diamond response reported in Ref. [55] does not show the strong orientation dependence shown by the results presented here.

### D. Relevance for inertial confinement fusion studies

Because diamond is an important ablator material in inertial confinement fusion (ICF) platforms [56,57], the findings presented here may have significance for the ICF effort. In particular, because numerical simulations are crucial for understanding the results of ICF-related high energy density physics experiments [58,59], accurate material models for ICF capsule materials, including diamond ablaters, are of critical importance. ICF-related simulations typically use tabular equation of state models for diamond that assume hydrodynamic response [59,60]. However, the findings presented here show that material models assuming hydrodynamic response cannot correctly describe the response of diamond shocked

to stresses below melt (as occurs in Ref. [61], for example). Therefore, although ICF capsules are fabricated from polycrystalline diamond and not diamond single crystals, the development of an accurate material description for diamond shocked to multimegabar stresses is clearly an important need.

Previous ICF-related work includes experiments where diamond ablators were shocked to stresses within the solid-liquid coexistence region [56,60]. This leads to an important question: Is diamond hydrodynamic when shocked to a solid-liquid mixed phase state? Experiments on diamond single crystals shocked along multiple crystal orientations, to stresses higher than those examined here, are needed to address this question.

## V. SUMMARY AND CONCLUSIONS

In previous studies, solids shocked to high stresses (above a Mbar) have typically been analyzed using the hydrodynamic approximation. Although this assumption may be reasonable for metals and many other solids at very high shock stresses, its validity for strong and stiff materials remains an open question. Because shock wave results for diamond, the archetypal strong solid, have often been analyzed assuming a hydrodynamic response [32–35], the present work was motivated by the following conceptual questions: at what stresses does the hydrodynamic assumption become a good approximation for diamond; how is crystal anisotropy manifested at multi-Mbar stresses in shocked diamond; and how to understand the inelastic response of diamond at these very high stresses?

Plate impact experiments were conducted to examine the elastic-inelastic response of [100]-, [110]-, and [111]-oriented diamond single crystals shocked to  $\sim 900$  GPa elastic impact stress. The main experimental findings from our work are summarized below.

(1) Two-wave structures (elastic-inelastic response) were observed for [110] and [111] diamond up to the highest stresses examined ( $\sim 900$  GPa EIS), which are likely at or near the melt stress. In contrast, single overdriven waves were observed for [100] diamond at 480 GPa EIS and above.

(2) The measured elastic wave speeds show strong orientation dependence; elastic wave velocities for the [110] and [111] orientations are significantly larger than those for the [100] orientation.

(3) Elastic wave amplitudes determined for [110] diamond are significantly larger than those for [100] and [111] diamond. In addition, the elastic wave amplitudes for [110] and [111] diamond increase significantly with increasing elastic impact stress.

The above findings provide important insight into the elastic-inelastic response of diamond single crystals shocked to high stresses. In particular, the two-wave structures observed for [110] and [111] diamond (but not for [100] diamond at 480 GPa and above) and the strong orientation dependence of the elastic wave speeds and elastic wave amplitudes demonstrate unequivocally that the hydrodynamic approximation is not valid for diamond single crystals shocked to stresses below melt.

The results presented here have focused mainly on the diamond elastic response. To rigorously analyze the inelastic deformation response and to characterize the peak state, nu-

merical simulations are required that incorporate an accurate material model for inelastic deformation in shock-compressed diamond single crystals. The development of such a model, though extremely challenging, is an important need. The experimental results presented here for diamond shocked along different crystal orientations provide an excellent foundation for such a development.

Having demonstrated that the archetypal strong solid, diamond, is not hydrodynamic at high (multi-Mbar) stresses, the present findings raise the following question: Is the nonhydrodynamic response at high stresses common to many strong brittle solids or is diamond a special case? To address this question, experiments are needed to measure wave profiles at high stresses for other strong solids.

## ACKNOWLEDGMENTS

C. McCoy at Sandia National Laboratories is gratefully acknowledged for assistance with the experiments. This work was supported by the U.S. Department of Energy (DOE), National Nuclear Security Administration (NNSA) under Award No. DE-NA0002007 and by Sandia National Laboratories under the Z Fundamental Science Program. Sandia National Laboratories is a multimission laboratory managed and operated by National Technology and Engineering Solutions of Sandia, LLC., a wholly owned subsidiary of Honeywell International, Inc., for the DOE/NNSA under Contract No. DE-NA0003525.

## APPENDIX: DETERMINATION OF SHOCK WAVE STRUCTURE FROM INTERFEROMETRY RESULTS

As mentioned in the main text, for experiments incorporating a LiF window, the measured wave profiles provide a direct indication of the shock wave structure; the elastic wave arrives first, imparting motion to the diamond/LiF interface, and the subsequent arrival of the inelastic wave further accelerates the interface (see Fig. 4). For experiments incorporating a quartz window, determination of the shock wave structure is not as direct due to the optical response of quartz. To determine the wave structure, we took advantage of the large difference in the refractive index of diamond and quartz (2.42 and 1.54 at 532 nm, respectively). When diamond and quartz are bonded together, this difference in refractive index leads to a Fresnel reflection of  $\sim 5\%$  at the diamond/quartz interface. Thus, a non-negligible fraction of the light returning to the VISAR interferometer from the sample location emanates from this interface.

To understand the role of this reflected light, consider first an experiment that results in a single overdriven wave in the diamond sample. At impact, most of the interferometry signal is lost due to shock-induced optical opacity in the diamond crystal; the signal that remains comes from the Fresnel reflection at the diamond/quartz interface. Upon arrival of the single overdriven wave at the diamond/quartz interface, the quartz is driven to a peak state of several hundred GPa. The shock front of quartz becomes reflective for strong shocks above  $\sim 100$  GPa [45]. Thus, arrival of the single overdriven wave at the diamond/quartz interface results in immediate recovery of

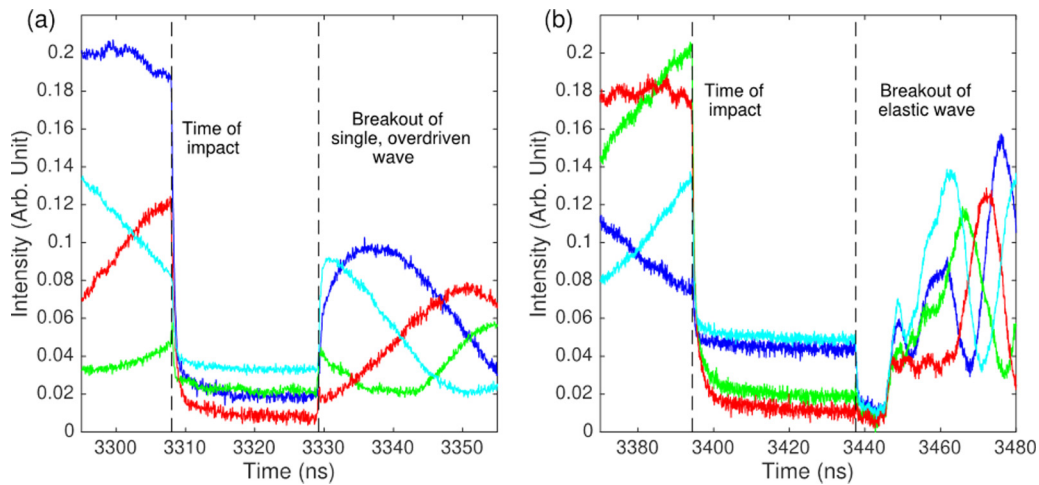


FIG. 9. Representative interferometry (VISAR) signals from a diamond sample backed by a quartz window for the case of (a) a single, overdriven wave in the diamond sample (Z3011-S3), and (b) a two-wave structure in the diamond (Z3029-N5).

the interferometry signal. Figure 9(a) shows a representative interferometry signal for this case.

Now consider an experiment that results in a two-wave structure (elastic-inelastic) in the diamond sample. Again, at impact most of the interferometry signal is lost due to shock-induced optical opacity in the diamond crystal. Because diamond has a much larger shock impedance than quartz (particularly in the case of elastically compressed diamond), arrival of the elastic wave at the diamond/quartz interface results in a transmitted shock in the quartz that is well below 100 GPa. For shocks above the elastic limit ( $\sim 6$  GPa) and below  $\sim 100$  GPa, quartz is observed to be optically opaque. This results in further loss of the interferometry signal; laser light no longer reaches the diamond/quartz interface. The subsequent inelastic wave drives a much stronger, several hundred GPa shock in the quartz window; this shock, which travels at a much higher Lagrangian wave speed, eventu-

ally overtakes the leading shock in the quartz, resulting in a reflecting shock front. Thus, in this case, additional loss of the interferometry signal corresponds to the arrival of an elastic wave at the diamond/quartz interface and recovery of the interferometry signal corresponds to coalescence of the two shocks in quartz to a single, large shock. Figure 9(b) shows a representative interferometry signal for this case.

Note that the arrival time of the second (inelastic) shock wave at the diamond/quartz interface is not directly measured in the above experiments. Therefore, the peak longitudinal stress reached by the two-wave loading process in the diamond samples cannot be determined directly from the experiments; numerical simulations using an accurate material description for diamond are required to analyze the quartz window data. The requisite material model is currently under development.

- [1] J. M. Walsh and R. H. Christian, *Phys. Rev.* **97**, 1544 (1955).
- [2] J. M. Walsh, M. H. Rice, R. G. McQueen, and F. L. Yarger, *Phys. Rev.* **108**, 196 (1957).
- [3] L. V. Al'tshuler, K. K. Krupnikov, B. N. Ledenev, V. I. Zhuchikhin, and M. I. Brazhnik, *Sov. Phys. JETP* **34**, 606 (1958).
- [4] L. V. Al'tshuler, K. K. Krupnikov, and M. K. Brazhnik, *Sov. Phys. JETP* **34**, 614 (1958).
- [5] R. G. McQueen and S. P. Marsh, *J. Appl. Phys.* **31**, 1253 (1960).
- [6] G. R. Fowles, *J. Appl. Phys.* **32**, 1475 (1961).
- [7] G. E. Duvall, in *Stress Waves in Anelastic Solids*, edited by H. Kolsky and W. Prager (Springer-Verlag, Berlin, 1964), p. 20.
- [8] J. W. Taylor, *J. Appl. Phys.* **36**, 3146 (1965).
- [9] R. A. Graham and J. R. Asay, *High Temp. High Press.* **10**, 355 (1978).
- [10] A. N. Dremin and G. A. Adadurov, *Sov. Phys. Solid State* **6**, 1379 (1964).
- [11] R. A. Graham, F. W. Neilson, and W. B. Benedick, *J. Appl. Phys.* **36**, 1775 (1965).
- [12] D. D. Keough and J. Y. Wong, *J. Appl. Phys.* **41**, 3508 (1970).
- [13] L. M. Barker and R. E. Hollenbach, *J. Appl. Phys.* **43**, 4669 (1972).
- [14] J. R. Asay, G. R. Fowles, G. E. Duvall, M. H. Miles, and R. F. Tinder, *J. Appl. Phys.* **43**, 2132 (1972).
- [15] D. E. Grady, W. J. Murri, and G. R. Fowles, *J. Geophys. Res.* **79**, 332 (1974).
- [16] J. N. Johnson, R. S. Hixson, G. T. Gray, and C. E. Morris, *J. Appl. Phys.* **72**, 429 (1992).
- [17] J. J. Dick and J. P. Ritchie, *J. Appl. Phys.* **76**, 2726 (1994).
- [18] G. I. Kanel, W. J. Nellis, A. S. Savinykh, S. V. Razorenov, and A. M. Rajendran, *J. Appl. Phys.* **106**, 043524 (2009).
- [19] R. Chau, J. Stolken, P. Asoka-Kumar, M. Kumar, and N. C. Holmes, *J. Appl. Phys.* **107**, 023506 (2010).
- [20] D. Choudhuri and Y. M. Gupta, *J. Appl. Phys.* **114**, 153504 (2013).
- [21] G. E. Duvall and R. A. Graham, *Rev. Mod. Phys.* **49**, 523 (1977).

- [22] W. J. Nellis, N. C. Holmes, A. C. Mitchell, and M. van Thiel, *Phys. Rev. Lett.* **53**, 1661 (1984).
- [23] S. T. Weir, A. C. Mitchell, and W. J. Nellis, *Phys. Rev. Lett.* **76**, 1860 (1996).
- [24] D. H. Kalantar, J. F. Belak, G. W. Collins, J. D. Colvin, H. M. Davies, J. H. Eggert, T. C. Germann, J. Hawreliak, B. L. Holian, and K. Kadau *et al.*, *Phys. Rev. Lett.* **95**, 075502 (2005).
- [25] R. F. Trunin, M. V. Panov, and A. B. Medvedev, *JETP Lett.* **62**, 594 (1995).
- [26] M. D. Knudson, D. L. Hanson, J. E. Bailey, C. A. Hall, J. R. Asay, and W. W. Anderson, *Phys. Rev. Lett.* **87**, 225501 (2001).
- [27] R. Nora, W. Theobald, R. Betti, F. J. Marshall, D. T. Michel, W. Seka, B. Yaakobi, M. Lafon, C. Stoeckl, and J. Delettrez, A. A. Solodov, A. Casner, C. Reverdin, X. Ribeyre, A. Vallet, J. Peebles, F. N. Beg, and M. S. Wei, *Phys. Rev. Lett.* **114**, 045001 (2015).
- [28] M. A. Meyers, H. Jarmakani, E. M. Bringa, and B. A. Remington, Dislocations in Shock Compression and Release, in *Dislocations in Solids*, edited by J. P. Hirth and L. Kubin (Elsevier, Amsterdam, 2009), Vol. 15, pp. 91–197.
- [29] G. T. Gray, *Annu. Rev. Mater. Res.* **42**, 285 (2012).
- [30] J. H. Nguyen and N. C. Holmes, *Nature (London)* **427**, 339 (2004).
- [31] S. Root, L. Shulenburg, R. W. Lemke, D. H. Dolan, T. R. Mattsson, and M. P. Desjarlais, *Phys. Rev. Lett.* **115**, 198501 (2015).
- [32] M. N. Pavlovskii, *Sov. Phys. Solid State* **13**, 741 (1971).
- [33] H. Nagao, K. G. Nakamura, K. Kondo, N. Ozaki, K. Takamatsu, T. Ono, T. Shiota, D. Ichinose, K. A. Tanaka, and K. Wakabayashi *et al.*, *Phys. Plasmas* **13**, 052705 (2006).
- [34] M. D. Knudson, M. P. Desjarlais, and D. H. Dolan, *Science* **322**, 1822 (2008).
- [35] R. F. Smith, J. H. Eggert, R. Jeanloz, T. S. Duffy, D. G. Braun, J. R. Patterson, R. E. Rudd, J. Biener, A. E. Lazicki, and A. V. Hamza *et al.*, *Nature (London)* **511**, 330 (2014).
- [36] J. M. Lang and Y. M. Gupta, *J. Appl. Phys.* **107**, 113538 (2010).
- [37] J. M. Lang, J. M. Winey, and Y. M. Gupta, *Phys. Rev. B* **97**, 104106 (2018).
- [38] K. Kondo and T. J. Ahrens, *Geophys. Res. Lett.* **10**, 281 (1983).
- [39] M. K. Matzen, M. A. Sweeney, R. G. Adams, J. R. Asay, J. E. Bailey, G. R. Bennett, D. E. Bliss, D. D. Bloomquist, T. A. Brunner, and R. B. Campbell *et al.*, *Phys. Plasmas* **12**, 055503 (2005).
- [40] R. Lemke, M. D. Knudson, and J.-P. Davis, *Int. J. Impact Eng.* **38**, 480 (2011).
- [41] W. F. Hemsing, *Rev. Sci. Instrum.* **50**, 73 (1979).
- [42] O. T. Strand, D. R. Goosman, C. Martinez, T. L. Whitworth, and W. W. Kuhlow, *Rev. Sci. Instrum.* **77**, 083108 (2006).
- [43] T. Ao and D. H. Dolan, *Rev. Sci. Instrum.* **82**, 023907 (2011).
- [44] P. A. Rigg, M. D. Knudson, R. J. Scharff, and R. S. Hixson, *J. Appl. Phys.* **116**, 033515 (2014).
- [45] D. G. Hicks, T. R. Boehly, J. H. Eggert, J. E. Miller, P. M. Celliers, and G. W. Collins, *Phys. Rev. Lett.* **97**, 025502 (2006).
- [46] C. A. McCoy, M. D. Knudson, and S. Root, *Phys. Rev. B* **96**, 174109 (2017).
- [47] D. K. Bradley, J. H. Eggert, D. G. Hicks, P. M. Celliers, S. J. Moon, R. C. Cauble, and G. W. Collins, *Phys. Rev. Lett.* **93**, 195506 (2004).
- [48] See Supplemental Material at <http://link.aps.org/supplemental/10.1103/PhysRevB.101.184105> for the following items requested by an anonymous referee: (1) comparison of elastic impact stresses for diamond single crystals with stress-volume curves determined for polycrystalline diamond, (2) wave profile calculations using a material model valid for isotropic metals, and (3) assessment of results from previous laser-shock experiments on diamond single crystals, see Refs. [62,63].
- [49] J. H. Eggert, D. G. Hicks, P. M. Celliers, D. K. Bradley, R. S. McWilliams, R. Jeanloz, J. E. Miller, T. R. Boehly, and G. W. Collins, *Nat. Phys.* **6**, 40 (2010).
- [50] J. M. Lang and Y. M. Gupta, *Phys. Rev. Lett.* **106**, 125502 (2011).
- [51] J. D. Clayton, *Int. J. Eng. Sci.* **79**, 1 (2014).
- [52] H. J. McSkimin and P. Andreatch, *J. Appl. Phys.* **43**, 2944 (1972).
- [53] J. M. Winey and Y. M. Gupta, *J. Appl. Phys.* **96**, 1993 (2004).
- [54] J. M. Winey and Y. M. Gupta, *J. Appl. Phys.* **99**, 023510 (2006).
- [55] R. S. McWilliams, J. H. Eggert, D. G. Hicks, D. K. Bradley, P. M. Celliers, D. K. Spaulding, T. R. Boehly, G. W. Collins, and R. Jeanloz, *Phys. Rev. B* **81**, 014111 (2010).
- [56] A. J. MacKinnon, N. B. Meezan, J. S. Ross, S. Le Pape, L. Berzak Hopkins, L. Divol, D. Ho, J. Milovich, A. Pak, and J. Ralph *et al.*, *Phys. Plasmas* **21**, 056318 (2014).
- [57] L. F. Berzak-Hopkins, N. B. Meezan, S. Le Pape, L. Divol, A. J. MacKinnon, D. D. Ho, M. Hohenberger, O. S. Jones, G. Kyrala, and J. L. Milovich *et al.*, *Phys. Rev. Lett.* **114**, 175001 (2015).
- [58] K. L. Baker, C. A. Thomas, D. T. Casey, S. Khan, B. K. Spears, R. Nora, T. Woods, J. L. Milovich, R. L. Berger, and D. Strozzi *et al.*, *Phys. Rev. Lett.* **121**, 135001 (2018).
- [59] D. S. Clark, A. L. Kritcher, S. A. Yi, A. B. Zylstra, S. W. Haan, and C. R. Weber, *Phys. Plasmas* **25**, 032703 (2018).
- [60] B. M. Haines, R. E. Olson, W. Sweet, S. A. Yi, A. B. Zylstra, P. A. Bradley, F. Elsner, H. Huang, R. Jimenez, and J. L. Kline *et al.*, *Phys. Plasmas* **26**, 012707 (2019).
- [61] O. L. Landen, D. K. Bradley, D. G. Braun, V. A. Smalyuk1, D. G. Hicks, P. M. Celliers, S. Prsbrey, R. Page, T. R. Boehly, and S. W. Haan *et al.* *J. Phys.: Conf. Ser.* **112**, 022004 (2008).
- [62] D. Orlikowski, A. A. Correa, E. Schwegler, and J. E. Klepeis, in *Shock Compression of Condensed Matter –2007*, edited by M. Elert, M. D. Furnish, R. Chau, N. Holmes, and J. Nguyen (AIP, New York, 2007), p. 247.
- [63] D. J. Steinberg, S. G. Cochran, and M. W. Guinan, *J. Appl. Phys.* **51**, 1498 (1980).